Autophagic flux without a block differentiates varicella-zoster virus infection from herpes simplex virus infection

Erin M. Buckingham[a], John E. Carpenter[a], Wallen Jackson[a], Leigh Zerboni[b], Ann M. Arvin[b], and Charles Grose[a,1]

[a]Virology Laboratory, Department of Pediatrics, University of Iowa Children's Hospital, Iowa City, IA 52242; and [b]Departments of Pediatrics and Microbiology and Immunology, Stanford University School of Medicine, Stanford, CA 94305

Autophagy is a process by which misfolded and damaged proteins are sequestered into autophagosomes, before degradation in and recycling from lysosomes. We have extensively studied the role of autophagy in varicella-zoster virus (VZV) infection, and have observed that vesicular cells are filled with >100 autophagosomes that are easily detectable after immunolabeling for the LC3 protein. To confirm our hypothesis that increased autophagosome formation was not secondary to a block, we examined all conditions of VZV infection as well as carrying out two assessments of autophagic flux. We first investigated autophagy in human skin xenografts in the severe combined immunodeficiency (SCID) mouse model of VZV pathogenesis, and observed that autophagosomes were abundant in infected human skin tissues. We next investigated autophagy following infection with sonically prepared cell-free virus in cultured cells. Under these conditions, autophagy was detected in a majority of infected cells, but was much less than that seen after an infected-cell inoculum. In other words, inoculation with lower-titered cell-free virus did not reflect the level of stress to the VZV-infected cell that was seen after inoculation of human skin in the SCID mouse model or monolayers with higher-titered infected cells. Finally, we investigated VZV-induced autophagic flux by two different methods (radiolabeling proteins and a dual-colored LC3 plasmid); both showed no evidence of a block in autophagy. Overall, therefore, autophagy within a VZV-infected cell was remarkably different from autophagy within an HSV-infected cell, whose genome contains two modifiers of autophagy, ICP34.5 and US11, not present in VZV.

autophagy | autophagosome | SCID-mouse | ICP34.5 | Epstein–Barr virus

VZV induces macroautophagy (hereafter referred to as autophagy) in skin cells within the typical exanthem associated with either primary VZV infection (varicella or chickenpox) or VZV reactivation (herpes zoster or shingles). During prior studies, the extent of autophagy was gauged by enumeration of autophagosomes by both 2D and 3D microscopy (1, 2). The usual number of autophagosomes seen by 3D animation was 100 per infected cell, but sometimes approached 200 per cell. In contrast, a typical nonstressed cell usually has fewer than 4 autophagosomes (3, 4). When monolayers were inoculated with VZV-infected cells, the traditional method for VZV infection, autophagy was again easily seen after enumeration of autophagosomes and immunoblotting for the LC3-phosphatidylethanolamine conjugate (LC3-II). Again these results suggested that autophagic flux was present during VZV infection in cultured cells.

As part of a more extensive assessment of autophagy after VZV-induced cellular stress, we have now investigated autophagy in infected human skin xenografts from the SCID mouse model of VZV infection. This model is the most accurate representation of the skin manifestation of varicella in the human host (5, 6). Finally, we addressed an important point about the nature of VZV-induced autophagy. Because the number of autophagosomes seen in the human vesicle cells from varicella

and herpes zoster patients is so high, the question has arisen whether there is a late block in the maturation of autophagosomes to autolysosomes. In this report, we demonstrate that (*i*) autophagy induced by VZV infection is related to the overall stress to the cell, namely, a higher inoculum leads to greater autophagy; and that (*ii*) autophagosomes induced during VZV infection mature into autolysosomes without an obvious block before final maturation. The autophagic flux assay results confirm that VZV infection induces autophagy that proceeds to completion, possibly allowing the cell to alleviate the cellular stress caused by the viral infection (7). In previous work, we showed that inhibition of autophagy led to a significant decrease in VZV titer. Overall, therefore, autophagy within a VZV-infected cell is remarkably different from autophagy within an HSV-infected cell, an alphaherpesvirus whose genome contains two modifiers of autophagy, ICP34.5 and US11 (8–13). In contrast, autophagy appears to be proviral in the life cycle of VZV.

Results

Autophagy in VZV-Infected Human Skin Xenografts in the SCID Mouse. VZV is renowned for its specificity to a limited number of human cell lines. Because of this restriction to human tissues, there is no animal model that completely mimics the human disease varicella. However, the SCID mouse model for VZV infection has provided the best alternative system to study the manifestations of VZV replication in the skin. In this model, human fetal skin xenografts are inserted beneath the skin of the

Significance

Varicella-zoster virus (VZV) is an important pathogen, which causes varicella and herpes zoster in humans. In general, there are similarities in virus-host interactions between the alphaherpesviruses. One notable exception is the response to autophagy. VZV infection induces autophagy. This is in contrast to herpes simplex virus (HSV), which has two genes that inhibit autophagy, ICP34.5 and US11; neither is present in the smaller VZV genome. In this study, we found that VZV-induced autophagic flux was not blocked. These results reinforce prior observations showing a proviral effect of autophagy on VZV infectivity and spread. These VZV findings also exhibit similarities with recent data about a requirement for early phase autophagy during Epstein–Barr virus infection, a phylogenetically distant gammaherpesvirus.

www.manaraa.com

severe combined immunodeficiency (SCID) mouse (14). In turn, replicate xenografts are inoculated with VZV-infected cells and then harvested at 7, 14, and 21 d after infection. This model system allows for the study of VZV infection of a differentiated human tissue in the context of no adaptive immune response. The pathology is remarkably similar to that seen in biopsies of vesicles during human varicella (5). To confirm and extend our autophagy investigations, therefore, we examined skin xenografts infected with VZV in vivo.

VZV-infected human skin was removed 21 d post infection and sections were stained with a monoclonal antibody to VZV glycoprotein E (gE), to identify infected areas of the tissue, as well as rabbit polyclonal antibody against LC3, to identify autophagosomes. The sections were examined by brightfield and confocal fluorescence microscopy. Images of complete serial sections are shown in Fig. 1. The brightfield image (Fig. 1*A*) shows evidence of major disruption of the tissue interior due to viral pathology. The fluorescent image (Fig. 1*B*) shows extensive VZV gE (red) expression throughout the tissue section, as well as LC3 expression, indicative of autophagosomes (green).

Examination of these fluorescently stained tissues at higher power, and analysis of Z stacks assembled into 3D projections using the Imaris imaging program confirmed that VZV infection in the SCID mouse model was associated with abundant autophagy. Fig. 2 *A*–*F* shows several representative images from these xenografts, with many LC3-positive puncta (green) seen in and near VZV-infected (red) cells. Mock infection of human tissue in the SCID mouse was also performed and analyzed by confocal microscopy. The skin tissue was intact (Fig. 2*G*) and

Fig. 2. VZV infection induces extensive autophagosome formation in human skin xenografts. (*A*–*F*) Sections from 21 dpi human skin xenografts were immunolabeled with MAb 3B3 (anti-VZV gE, red) and anti-LC3 antibody [Santa Cruz (*A*–*E*) or Epitomics (*F*), green] primary antibodies as well as H33342 (DNA stain, blue). Z-stack images were analyzed using the Imaris software to create 3D reconstructions that show LC3-positive autophagosomes as green spots and nuclei as blue spots. Abundant autophagosomes are noted in both samples. gE staining (red) is displayed flat to show diffuse and abundant staining in infected cells, often most highly concentrated in the ER/Golgi. Images shown are from either 400× total magnification (*A* and *B*) or 630× total magnification (*C*–*F*). (*G*–*I*) These three images each show a single fluorescent channel of the same 2D confocal image of mock infected human skin implants from a SCID-hu mouse at 630× total magnification. Mock infection showed no gE staining (*I*) and minimal LC3 staining (*H*).

there was very minimal LC3 staining present (Fig. 2*H*) and no VZV gE expression (Fig. 2*I*). In summary, abundant autophagy was evident in the VZV-infected skin xenograft.

Comparison of Autophagy in the VZV-Infected Skin Xenografts with Human Vesicles. In early experiments, we documented the presence of autophagosomes in skin vesicles from immunocompetent children with varicella or adults with herpes zoster (15, 16). To confirm that the autophagy seen in the VZV-infected skin xenografts in SCID mice, which lack adaptive immune responses, recapitulated the response seen in human skin vesicles from children with varicella, we performed a direct comparison. As can be seen by viewing Fig. 3 *A* and *B*, the pattern and distribution of LC3-positive (green) autophagosomes were similar in the two samples. Together, these data again demonstrated the validity of the SCID mouse model to recapitulate pathogenesis in human skin infected VZV during varicella or herpes zoster.

Autophagy After High Input Cell-Free Virus Inoculation. VZV assembly in infected cells is an extremely labile process. In contrast to HSV, complete enveloped virions are not released from infected cells. Instead, VZV-infected cells are sonically disrupted to release what is called cell-free virus. The titer of this product is very low; the estimated particle to PFU ratio was 40,000:1 (17). To expand our knowledge about the role of input inoculum on the subsequent induction of autophagy in VZV-infected cells, we postulated that inoculation of cells with cell-free virus would lead to lower levels of autophagy than seen in the human vesicle or
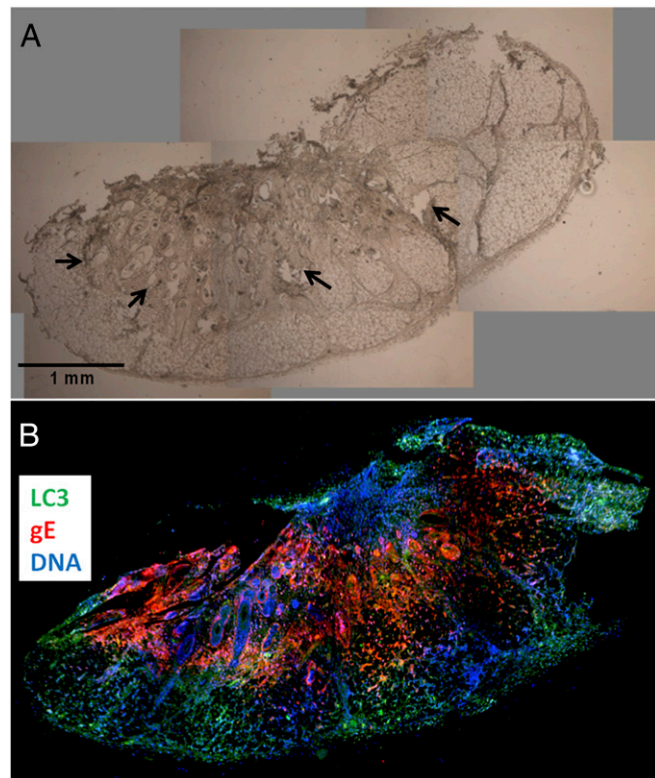

Fig. 1. VZV induces extensive LC3 puncta indicative of autophagosomes in human skin cells in the xenografts in the SCID mouse model. VZV-infected human skin xenografts at 21 dpi were immunolabeled with antibodies to VZV gE (red) and to LC3 (green), as well as the Hoescht 33342 DNA stain (blue). Brightfield (*A*) and fluorescent (*B*) images of successive, whole sections of human skin xenografts showed extensive disruption of the tissue with prominent VZV gE expression as well as LC3 staining of autophagosomes. Areas of tissue disruption caused by VZV infection in *A* are noted by arrows.
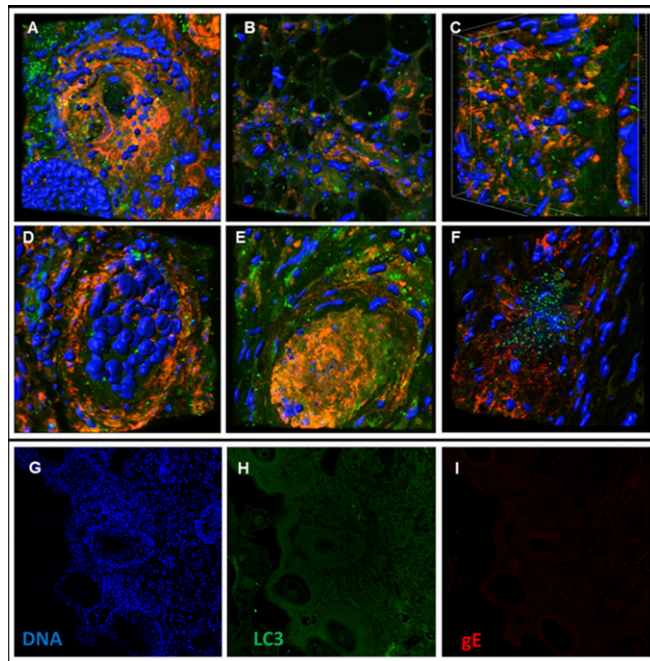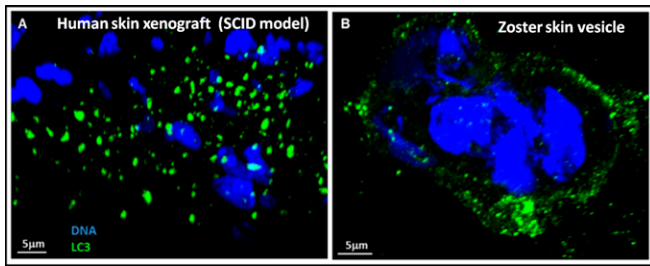
www.manaraa.com

Fig. 3. VZV infection induces comparable autophagy in human skin and in a SCID mouse model. This comparison included 3D reconstructions of confocal microscopy images of a VZV-infected (21 dpi) human skin xenograft from a SCID mouse (*A*) and an impression of cells from a skin vesicle of a zoster patient (*B*). Both samples were immunolabeled with antibodies against LC3 (green) as well as a DNA stain (H33342, blue). Z-stack images at 630× total magnification were analyzed using the Imaris software to create 3D reconstructions that show LC3-positive autophagosomes as green spots and nuclei as blue spots. Abundant autophagosomes were noted in both samples. The gE staining (red) is displayed flat to show diffuse and abundant staining in infected cells, often most highly concentrated in the ER/Golgi.

after inoculation with infected cells. In an initial set of experiments, the inoculum was a relatively high input of cell-free virus.

MRC-5 fibroblasts were infected with 1600 pfu per 10 cm². Labeled gE was detected at 48 hpi, but wasn't widespread until 72–96 hpi (Fig. 4). As expected, spread of infection after using cell-free virus occurred at a much slower rate than is typically seen during cell-associated infection. However, LC3 puncta were evident at early times postinfection, at 6 and 12 hpi (Fig. 4A1-A4.) Percentages of LC3-positive cells were significantly higher in VZV-infected cultures than in mock infected cultures (Fig. 4*B*) at these early times postinfection. (**6 h, $P < 0.008$; *$P < 0.024$; **24 h, $P < 0.001$; $n \geq 9$ images). When MRC-5 fibroblasts were infected with an even lower titer (400 pfu per 10 cm²), very few LC3 puncta were seen (Fig. S1*A*). We also performed quantitative analyses of LC3-positive cells in infected versus uninfected cells. Significantly more infected cells were LC3-positive than uninfected cells (Fig. 4*C*; *$P < 0.033$; **$P < 0.001$; ***$P \leq 0.0001$; $n = 10$ images). This result indicated that most autophagy seen in an infected culture was within the infected cells themselves.

During the above studies, we observed several differences in antigen detection between our microscopy data and results already published (18). However, under permeabilization conditions with high amounts of Triton X-100, we detected gE at earlier timepoints than with low amounts of permeabilization (Fig. S2). The above experiments to enumerate LC3 puncta after infection with cell-free virus demonstrated that this method of infection did not lead to the levels of autophagy seen in human skin vesicles, in VZV-infected skin xenografts in the SCID mouse model, or in monolayers inoculated with infected cells.

Autophagy Within an Infectious Focus After Cell-Free Virus Inoculation. After inoculation with cell-free virus, several small infectious foci appear in the monolayer over the first 72 hpi. At 72 and 96 hpi, monolayers were fixed, permeabilized, and immunolabeled for LC3 and VZV gE (Fig. 5 *A* and *B*). We observed LC3 puncta within cells at all stages of infection with cell-free virus, similar to what we had noted for cell-associated infection (1). When cells were categorized by ranges of number of LC3 puncta, we found more cells with higher numbers of puncta in the infected cells of a culture compared with the uninfected cells of the same culture (Fig. 5*C*). When looking at the overall level of stress in a cell after cell-free VZV infection, as illustrated by the presence of greater than four LC3 puncta per cell, there were a significantly higher number of highly stressed infected cells than uninfected cells in the same cultures (Fig. 5*D*; ***$P < 0.007$). These data indicated that infection within a single cell gradually led to a similar level of autophagy within the expanding infectious foci, compared with an infected cell inoculum.

Documentation of Autophagic Flux Following VZV Infection by Radiolabeling. In the next set of experiments, we postulated that the large number of autophagosomes seen in both human vesicle cells as well as in the VZV-infected human skin xenografts in the SCID mouse did not represent a blockade in the transition of autophagosomes into the lysosomal degradation pathway but instead represented a heightened autophagosomal response that progressed to completion. To test this hypothesis, we followed the guidelines outlined by Klionsky and coauthors: a traditional method by which to increase the specificity of autophagy assays is to use a pulse-chase radiolabeling technique, by which to measure the degradation of long-lived structural proteins that is termed autophagic flux (19). To carry out these studies, we performed pulse-chase experiments with amino acids radiolabeled with ³⁵S-Methionine/Cysteine (Met/Cys). In this
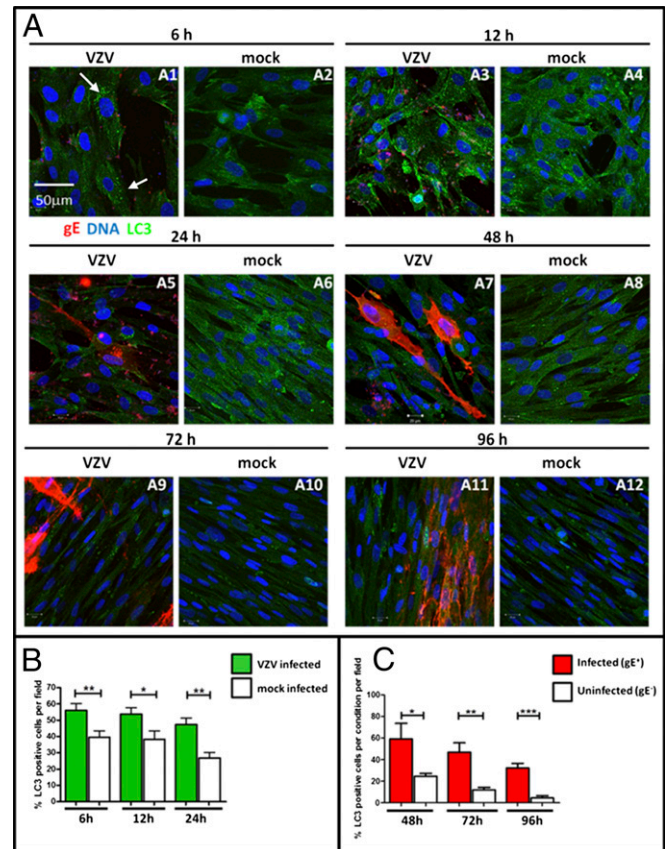

Fig. 4. Cell-free VZV infection of fibroblasts leads to autophagosome formation at early times post infection. MRC-5 cells were infected with a high input of cell free VZV-32 or were mock infected. Infected cells were fixed and permeabilized at 6, 12, 24, 48, 72, and 96 hpi, and stained with antibodies against VZV gE (red) and LC3 (green), as well as a DNA stain (blue). Samples were viewed by confocal microscopy. (*A*) Representative images of cells at each time point, both mock and VZV-infected. Arrows in panel A1 point to typical cells scored as LC3 positive due to the presence of four or more LC3 puncta. Images shown are 400× total magnification. (Scale bar, 50 μm.) (*B*) Quantitative analysis of LC3 positive cells per field. Confocal images were viewed in ImageJ and LC3-positive cells were identified as cells that contained four or more LC3 puncta. There were significantly more LC3-positive cells in the infected cultures than in the mock cultures. (**6 h, $P < 0.008$; *$P < 0.024$; **24 h, $P < 0.001$; $n \geq 9$ images). (*C*) Quantitative analysis of LC3-positive cells in infected versus uninfected cells within the VZV-infected cultures. Confocal microscopy images of cells from VZV-infected cultures at 48, 72, and 96 hpi were analyzed using ImageJ. Cells were labeled as infected if they were gE-positive by immunolabeling and uninfected if they contained no gE. Significantly more infected cells were LC3-positive than uninfected cells. (*$P < 0.033$; **$P < 0.001$; ***$P \leq 0.0001$; $n = 10$ images.)
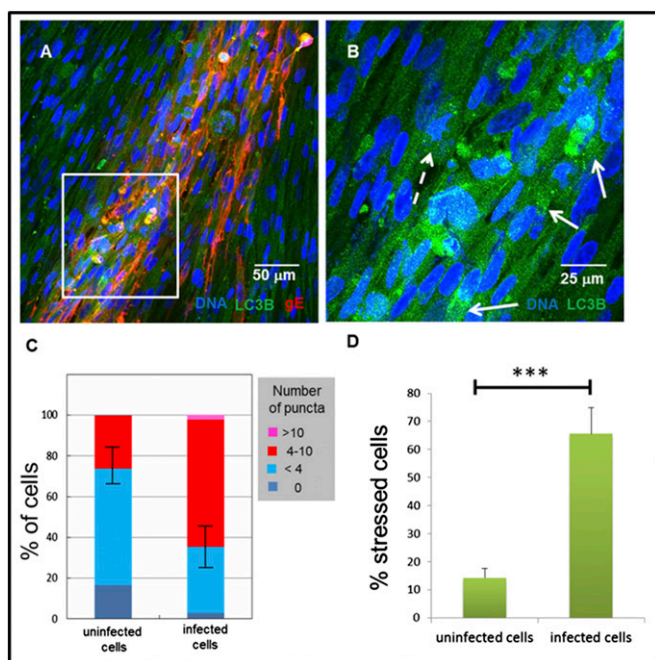
Buckingham et al.

www.manaraa.com

Fig. 5. Individual cells within a focus of infection after cell-free VZV infection exhibited LC3 puncta similar to cells infected with cell-associated VZV. MRC-5 cells were infected with a high-input of cell-free VZV-32 and fixed at 72 and 96 hpi. (*A*) Infected cells at 72 hpi (VZV gE; red) are apparent in the representative image at 400×. (*B*) Higher magnification (800×) images showing LC3 (green) in the area outlined by the white rectangle in panel A. Representative LC3 puncta indicative of autophagosomes are indicated by solid white arrows; similar puncta in a newly infected cell are indicated by a dashed white line. (*C*) Stacked bar chart showing the percentage of cells with a given number of LC3 puncta for both uninfected cells and infected cells from cultures infected with cell free VZV for 72–96 h. Blue colors indicate levels of puncta in unstressed cells, whereas red and pink colors indicate levels of puncta in stressed cells. (*D*) Different presentation of data from panel C, showing percent of stressed cells (cells that contain four or more LC3 puncta) in populations of uninfected (no gE staining) or infected (gE positive) cells. Cells infected with cell-free VZV exhibited more LC3 puncta indicative of autophagosomes than uninfected cells (***P < 0.007) and at levels similar to cells infected with cell-associated virus (1).

experiment, monolayers of uninfected cells and VZV-infected cells were pulse labeled for 2 h and then chased with unlabeled medium for 24 h. By scintillation counting, we determined that ~35% of the radiolabeled Met/Cys was taken up by the cells during the pulse period and that ~7% of that amount was expelled into the medium in the first 2 h of chase. This percentage corresponded to degradation of short-lived proteins by proteasomes. Another 7% of the absorbed fraction was expelled into the medium during the chase period from 2–24 h, corresponding to degradation of longer lived structural proteins.

To determine the contribution of autophagy to the degradation of longer lived proteins, Klionsky at al (19). recommended that half of the monolayers for each experiment receive treatment with 3-methyladenine (3-MA), an inhibitor of class I and class III phosphoinositide 3-kinase (PI3K) (20–22). Given that over 80% of the radiolabel was retained in the cells during the chase, we chose to measure the degradation rate by densitometry of lysates removed and saved during the chase period. In general, protein bands became lighter during the chase period due to degradation (Fig. 6). This effect was quantitated using mean pixel values measured with ImageJ. The difference between untreated cells and 3-MA-treated cells was revealed by subtracting the pulse value from each chase value to arrive at a "darkness" value. As expected, the degradation rate in uninfected fibroblast cells (Fig. 6*A*, lanes 3–5 vs. lanes 6–8) was

insensitive to 3-MA treatment, indicating that the base rate of −0.3 darkness/h is primarily proteasomal. VZV-infected cells generated a higher degradation rate (−0.64 darkness/h) than uninfected cells (Fig. 6*B*). Treatment with 3-MA dramatically lowered the degradation rate of VZV infected cells (to −0.13 darkness/h; Fig. 6*B*, lanes 3–5, without 3-MA vs. lanes 6, 7, 8 with 3-MA), a result indicating that the majority of the degradation of longer-lived proteins in VZV-infected cells was due to autophagy.

Documentation of Autophagic Flux with a Dual-Colored LC3 Plasmid. To confirm and expand the above results, we obtained the mRFP-GFP tandem fluorescent-tagged LC3 plasmid (ptfLC3). This plasmid contains both red and green fluorescent proteins tagged to the LC3 protein. During the process of autophagy, autophagosomes fuse with lysosomes to form autolysosomes, which provides an acidic environment and proteases for the degradation of the contents of the autophagosome. The autolysosome is distinguished from an autophagolysosome, which is a compartment that is specific to the process of xenophagy (23). It has been found that the fluorescent signal from GFP is quenched in an acidic environment of the lysosome, whereas the signal from mRFP remains intact (24). Thus, in autophagosomes, there will be yellow signals (overlap of red and green fluorescence) whereas the green signal is lost as the autophagosome fuses with the more acidic lysosome (24). Therefore, autolysosomes appear with red fluorescent LC3.

MRC-5 fibroblasts were transfected with the tandem fluorescent tagged LC3 plasmid (ptfLC3) and subsequently inoculated with VZV-infected cells at 48 h posttransfection. At 72 h postinfection (hpi), cells were fixed and stained with an antibody against VZV gE (white). Samples were examined by confocal microscopy and Z-stacks of images were analyzed using Imaris software for 3D reconstruction. A representative 3D image reconstruction is shown in Fig. 7. LC3 puncta were visible in infected cells. Spheres that are green and red (yellow arrow) represent autophagosomes that have not yet fused with lysosomes. Spheres that are red represent autolysosomes. Many images were analyzed with similar patterns of the presence of both red puncta as well as green and red puncta in infected cells, indicating that autophagic flux was intact in VZV-infected cells. These data confirmed our previous results that autophagy proceeded to completion in VZV infection. VZV infection did not cause a block in autophagic flux.

Discussion

The role of autophagy during HSV-1 infection has been found to involve two viral proteins, ICP34.5 and US11. The initial discovery about the role of ICP34.5 was brought to the forefront by Orvedahl et al., who demonstrated that this neurovirulence protein bound to the autophagy protein Beclin 1, the mammalian ortholog of yeast Atg6 (9). Beclin 1 interacts with several autophagy cofactors, to regulate and promote formation of the Beclin 1–Vps34–Vps15 complexes (22, 25). A domain within amino acids 68–87 of ICP34.5 interacts with Beclin 1 and thereby inhibits its ability to induce autophagy (9). Deletion of the ICP34.5 gene from the HSV long repeat region leads to increased autophagy in infected animals and decreased neurovirulence (9, 26). Subsequently, Lussignol et al. investigated the role of HSV US11 and confirmed that US11 also inhibited autophagy but via a mechanism independent of inhibition of Beclin 1 (13). What is important for interpretation of our study of VZV-induced autophagy is the fact that very few alphaherpesvirus genomes except for HSV-1 and HSV-2 have the ICP34.5 gene (27–30). In addition, many such as VZV lack an ortholog of US11 (31). VZV with the smallest herpesvirus genome, therefore, has discarded US11 (or never acquired it) and never captured the ICP34.5/GADD34-homolog gene during its evolution (32).

However, the VZV genome has retained the HSV ICP0 ortholog, ORF61. Infection of differentiated skin cells within their tissue microenvironment as observed using xenografts in SCID mice has revealed a dramatic up-regulation of the type I
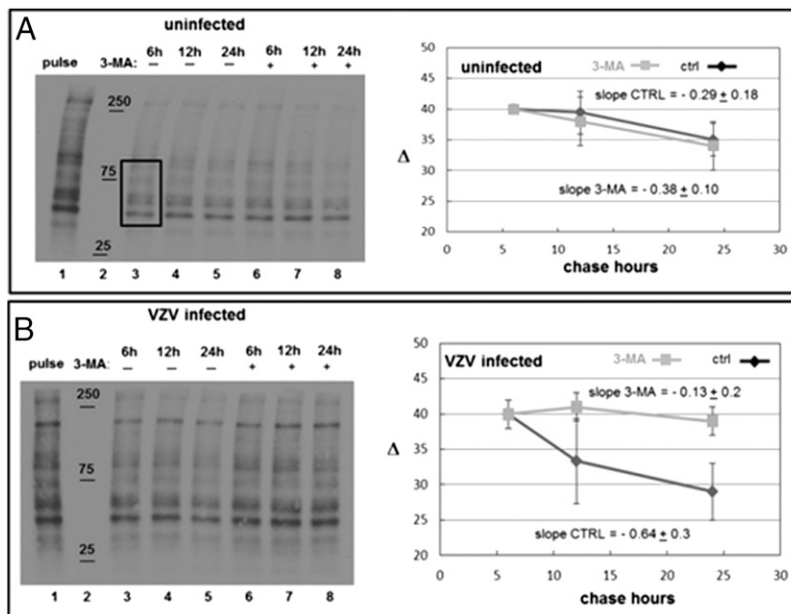
MICROBIOLOGY

Fig. 6. Autophagic flux during VZV infection of fibroblasts. VZV-infected monolayers (by cell-associated virus) were pulse labeled with ^{35}S-labeled Met/Cys and then lysates saved at chase times 6, 12, and 24 h with and without 3-MA treatment. Reduced lysates at all pulse and chase time points were electrophoresed, transferred to PVDF membranes, and exposed to film. The darkness of a selected area of each lane was measured with ImageJ and plotted relative to the pulse value. The procedure was duplicated three times. (A) Uninfected MRC-5 cells. 3-MA treatment made little difference to the overall rate of degradation in uninfected cells. The area used to measure pixel density is shown as a box. (B) VZV-infected cells. 3-MA treatment significantly decreased protein degradation in VZV-infected cells, indicating increased autophagic flux in infected cells.

IFN response in uninfected cells surrounding the VZV lesion, associated with STAT1 activation and enhanced numbers of promyelocytic protein (PML) nuclear bodies (33, 34). In contrast, VZV-infected cells show disruption of these innate antiviral mechanisms in an ORF61-dependent manner. Conversely, VZV infection induces STAT3 activation, leading to survivin expression, which is necessary for viral replication; inhibiting this pathway severely impairs VZV replication in skin (35). The finding that autophagic flux is maintained in VZV-infected skin cells suggests that this process may also represent a virus-cell interaction that has important proviral effects in vivo.

We had previously investigated VZV autophagic flux by measurement of stress-inducible intracellular p62/SQSTM1 protein levels in infected cells, and showed that VZV-induced autophagy was completed, leading to the degradation of p62/SQSTM1 (15). To confirm and extend our observations, we measured autophagic flux by a traditional pulse-chase assay using radiolabeled amino acids. This assay measures the turnover of long-lived proteins leading to a determination of autophagic flux. It is a well established methodology that is highly quantifiable, and is a recommended method in the "Guidelines for the use and interpretation of assays for monitoring autophagy" by Klionsky and colleagues (36). This assay showed that long-lived proteins were degraded by VZV-induced autophagy.
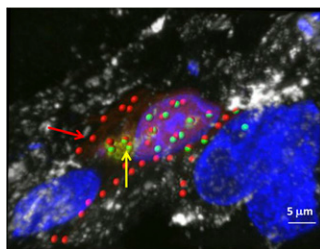

Fig. 7. Analysis of autophagic flux with a tandem red/green fluorescent protein-tagged LC3 plasmid. MRC-5 cells transfected with the tandem fluorescent tagged LC3 plasmid were inoculated with VZV-infected cells for 72 h then immunolabeled. Samples were examined by confocal microscopy, and analyzed with Imaris software for 3D reconstruction. LC3 puncta are illustrated by spheres that are green and red (yellow arrow), showing LC3 expression in autophagosomes, or red only (red arrow), showing LC3 expression in autolysosomes, where GFP fluorescence has been extinguished. Nuclei (blue), VZV gE (white). (Scale bar, 5 μm.)

We also investigated autophagic flux in VZV-infected cells using the mRFP-GFP tandem fluorescent-tagged LC3 plasmid (ptfLC3) created by Yoshimori and colleagues (24). This innovative plasmid has been used by other groups studying autophagy, to demonstrate the completion of autophagy by the formation of autolysosomes, such as in a study of HIV from Levine and colleagues (37). They used the ptfLC3 plasmid to show that siRNA knockdown of GAPR-1, a newly identified inhibitor of autophagy, increased autophagosome formation by causing an increase in autophagic flux rather than a block in autophagosome maturation. Another group studied of the role of autophagy in Newcastle Disease Virus (NDV) infection (38). This study showed that NDV infection induces autophagic flux in two different kinds of chicken cells. Also, the previously mentioned study by Lussignol et al. used ptfLC3-transfected HeLa cells to show that the HSV-1 protein US11 blocked autophagic flux to a similar degree as HSV-1 ICP34.5 (13). All of these studies together highlight the utility of the tandem fluorescent LC3 plasmid in the study of autophagic flux in virus systems. Once again, VZV is found to have a very different relationship with autophagy than the closely related alphaherpesvirus HSV-1, which has been shown to inhibit autophagy in several ways, including blocking autophagosome maturation (9, 12). Instead, the level of induction of autophagy by VZV is similar to that of known chemical inducers of autophagy, such as trehalose and tunicamycin (1).

Finally, the discussion about the proviral effects of autophagy during herpesvirus infection can now be extended beyond alphaherpesviruses based on an insightful report on the gamma-1 herpesvirus, Epstein–Barr virus (EBV) (39). Although EBV blocks autophagic flux during its replication cycle, the autophagic machinery is then usurped by EBV for transport of viral particles. Specifically, early phases of autophagic flux are required for the production of infectious EBV particles, whereas the late phase of autophagic flux (autolysosome formation) was blocked. Via this strategy, EBV redirects the expanding autophagic machinery that is reacting to the stress induced by viral infection toward the production of EBV particles. Thus, in a broader sense, autophagy is proviral in that autophagic components are used during the EBV replication cycle. As cited above, VZV being the herpesvirus with the smallest lacks the viral genes that inhibit the late phases of flux. Otherwise stated, of the 8 genes in the HSV-1 genome (152 kbp) not found in the VZV genome (124 kbp), two inhibit autophagy. Instead, VZV accommodates its replication cycle within an infected cell and its titer, similar to

Buckingham et al.

EBV, declines when autophagy is inhibited with either siRNA or 3-methyladenine (3-MA) (1). Thus, autophagy provides a link between two of the most phylogenetically divergent human herpesviruses: alpha VZV and gamma EBV.

Materials and Methods

More detailed experimental information is provided in *SI Materials and Methods*.

Viruses and Cells. VZV-32 is a low passage laboratory strain; its genome has been completely sequenced and falls within European clade 1 of VZV genotypes (40). Skin explants were infected with the parental rOka strain as in ref. 5. MRC-5 human fibroblast cells and MeWo strain of human melanoma cells were grown as in Grose and Brunel (41).

Generation of Cell-Free VZV or Uninfected Cell Sonicate. Three 25-cm^2 MeWo monolayers were infected at 1:8 infected: uninfected ratio and incubated at 32 °C for 72 h. The infected monolayers were scraped into 2 mL of SPA media (0.2 M sucrose, 0.01 M sodium phosphate, 1% BSA pH 7.4) and sonicated on ice for 20 s. The sonicate was centrifuged at 300 × *g* for 10 min at 4 °C. The pellet was discarded and the supernatant was diluted with 75 mL of complete MEM and added to 24 wells on six-well plates (3 mL per well).

VZV Infection of Human Skin Xenografts. Construction of human skin xenografts in SCID mice and subsequent inoculation with VZV or mock-infected cells was done as described (5, 42).

Primary and Secondary Antibody Reagents. Primary antibodies required for this study included the previously described VZV-specific murine monoclonal antibody (MAb) 3B3 and 370 (gE; ORF68; 1:1,000). Also used was a rabbit polyclonal antibody to MAP1LC3B (1:200: sc-28266, Santa Cruz Biotechnology), and a rabbit MAb anti-LC3A/B (1:1,000; 2057-1, Epitomics). Secondary antibodies used were AlexaFluor 488 and 546 fluoroprobes conjugated to goat anti-rabbit IgG or goat anti-mouse IgG F(ab')$_2$ fragment (1:1,250; Invitrogen).

Imaging Protocols. Samples of infected and uninfected cells were immuno-labeled and prepared for confocal microscopy by methods described previously (1, 2, 16).

Transfections of Cells with Tandem Fluorescent LC3 Plasmid. MRC-5 fibroblasts were transfected with the tandem fluorescent tagged LC3 plasmid (ptfLC3, Plasmid#21074 from Addgene.org; created by T. Yoshimori), as in ref. 24. After 24 h, the monolayer was inoculated with VZV-infected cells.

Protein Degradation Measurement by Pulse-Chase Radiolabeling. The basic experimental protocol is described in the autophagy literature (19) and our procedure is modeled on that used by Isler et al. (43). The 3-MA methodology has been described (1).

1. Buckingham EM, Carpenter JE, Jackson W, Grose C (2014) Autophagy and the effects of its inhibition on varicella-zoster virus glycoprotein biosynthesis and infectivity. J Virol 88(2):890–902.
2. Jackson W, Yamada M, Moninger T, Grose C (2013) Visualization and quantitation of abundant macroautophagy in virus-infected cells by confocal three-dimensional fluorescence imaging. J Virol Methods 193(1):244–250.
3. Kabeya Y, et al. (2000) LC3, a mammalian homologue of yeast Apg8p, is localized in autophagosome membranes after processing. EMBO J 19(21):5720–5728.
4. Tra T, et al. (2011) Autophagy in human embryonic stem cells. PLoS ONE 6(11):e27485.
5. Moffat JF, et al. (1998) Attenuation of the vaccine Oka strain of varicella-zoster virus and role of glycoprotein C in alphaherpesvirus virulence demonstrated in the SCID-hu mouse. J Virol 72(2):965–974.
6. Ku CC, Besser J, Abendroth A, Grose C, Arvin AM (2005) Varicella-Zoster virus pathogenesis and immunobiology: New concepts emerging from investigations with the SCIDhu mouse model. J Virol 79(5):2651–2658.
7. Carpenter JE, Grose C (2014) Varicella-zoster virus glycoprotein expression differentially induces the unfolded protein response in infected cells. Front Microbiol 5:322.
8. Chou J, Kern ER, Whitley RJ, Roizman B (1990) Mapping of herpes simplex virus-1 neurovirulence to gamma 134.5, a gene nonessential for growth in culture. Science 250(4985):1262–1266.
9. Orvedahl A, et al. (2007) HSV-1 ICP34.5 confers neurovirulence by targeting the Beclin 1 autophagy protein. Cell Host Microbe 1(1):23–35.
10. Alexander DE, Ward SL, Mizushima N, Levine B, Leib DA (2007) Analysis of the role of autophagy in replication of herpes simplex virus in cell culture. J Virol 81(22):12128–12134.
11. English L, et al. (2009) Autophagy enhances the presentation of endogenous viral antigens on MHC class I molecules during HSV-1 infection. Nat Immunol 10(5):480–487.
12. Gobeil PA, Leib DA (2012) Herpes simplex virus γ34.5 interferes with autophagosome maturation and antigen presentation in dendritic cells. MBio 3(5):e00267–e12.
13. Lussignol M, et al. (2013) The herpes simplex virus 1 Us11 protein inhibits autophagy through its interaction with the protein kinase PKR. J Virol 87(2):859–871.
14. Zerboni L, Sen N, Oliver SL, Arvin AM (2014) Molecular mechanisms of varicella zoster virus pathogenesis. Nat Rev Microbiol 12(3):197–210.
15. Takahashi MN, et al. (2009) Varicella-zoster virus infection induces autophagy in both cultured cells and human skin vesicles. J Virol 83(11):5466–5476.
16. Carpenter JE, Jackson W, Benetti L, Grose C (2011) Autophagosome formation during varicella-zoster virus infection following endoplasmic reticulum stress and the unfolded protein response. J Virol 85(18):9414–9424.
17. Carpenter JE, Henderson EP, Grose C (2009) Enumeration of an extremely high particle-to-PFU ratio for Varicella-zoster virus. J Virol 83(13):6917–6921.
18. Reichelt M, Brady J, Arvin AM (2009) The replication cycle of varicella-zoster virus: Analysis of the kinetics of viral protein expression, genome synthesis, and virion assembly at the single-cell level. J Virol 83(8):3904–3918.
19. Klionsky DJ (2008) Getting into the flow. Autophagy 4(2):139–140.
20. Wu YT, et al. (2010) Dual role of 3-methyladenine in modulation of autophagy via different temporal patterns of inhibition on class I and III phosphoinositide 3-kinase. J Biol Chem 285(14):10850–10861.
21. Seglen PO, Gordon PB (1982) 3-Methyladenine: Specific inhibitor of autophagic/lysosomal protein degradation in isolated rat hepatocytes. Proc Natl Acad Sci USA 79(6):1889–1892.
22. Funderburk SF, Wang QJ, Yue Z (2010) The Beclin 1-VPS34 complex—at the crossroads of autophagy and beyond. Trends Cell Biol 20(6):355–362.
23. Klionsky DJ, Eskelinen EL, Deretic V (2014) Autophagosomes, phagosomes, autolysosomes, phagolysosomes, autophagolysosomes... wait, I'm confused. Autophagy 10(4):549–551.
24. Kimura S, Noda T, Yoshimori T (2007) Dissection of the autophagosome maturation process by a novel reporter protein, tandem fluorescent-tagged LC3. Autophagy 3(5):452–460.
25. Furuya N, Yu J, Byfield M, Pattingre S, Levine B (2005) The evolutionarily conserved domain of Beclin 1 is required for Vps34 binding, autophagy and tumor suppressor function. Autophagy 1(1):46–52.
26. Bolovan CA, Sawtell NM, Thompson RL (1994) ICP34.5 mutants of herpes simplex virus type 1 strain 17syn+ are attenuated for neurovirulence in mice and for replication in confluent primary mouse embryo cell cultures. J Virol 68(1):48–55.
27. Davison AJ, Scott JE (1986) The complete DNA sequence of varicella-zoster virus. J Gen Virol 67(Pt 9):1759–1816.
28. Ravi V, Kennedy PG, MacLean AR (1998) Functional analysis of the herpes simplex virus type 2 strain HG52 RL1 gene: The intron plays no role in virulence. J Gen Virol 79(Pt 7):1613–1617.
29. Tang S, Guo N, Patel A, Krause PR (2013) Herpes simplex virus 2 expresses a novel form of ICP34.5, a major viral neurovirulence factor, through regulated alternative splicing. J Virol 87(10):5820–5830.
30. Guliani S, et al. (2002) Macropodid herpesvirus 1 encodes genes for both thymidylate synthase and ICP34.5. Virus Genes 24(3):207–213.
31. Cohen JI (2010) The varicella-zoster virus genome. Curr Top Microbiol Immunol 342:1–14.
32. Grose C (2012) Pangaea and the Out-of-Africa Model of Varicella-Zoster Virus Evolution and Phylogeography. J Virol 86(18):9558–9565.
33. Ku CC, et al. (2004) Varicella-zoster virus transfer to skin by T Cells and modulation of viral replication by epidermal cell interferon-alpha. J Exp Med 200(7):917–925.
34. Wang L, et al. (2011) Disruption of PML nuclear bodies is mediated by ORF61 SUMO-interacting motifs and required for varicella-zoster virus pathogenesis in skin. PLoS Pathog 7(8):e1002157.
35. Sen N, et al. (2012) Signal transducer and activator of transcription 3 (STAT3) and survivin induction by varicella-zoster virus promote replication and skin pathogenesis. Proc Natl Acad Sci USA 109(2):600–605.
36. Klionsky DJ, et al. (2012) Guidelines for the use and interpretation of assays for monitoring autophagy. Autophagy 8(4):445–544.
37. Shoji-Kawata S, et al. (2013) Identification of a candidate therapeutic autophagy-inducing peptide. Nature 494(7436):201–206.
38. Sun Y, et al. (2014) Autophagy benefits the replication of Newcastle disease virus in chicken cells and tissues. J Virol 88(1):525–537.
39. Granato M, et al. (2014) Epstein-barr virus blocks the autophagic flux and appropriates the autophagic machinery to enhance viral replication. J Virol 88(21):12715–12726.
40. Peters GA, et al. (2006) A full-genome phylogenetic analysis of varicella-zoster virus reveals a novel origin of replication-based genotyping scheme and evidence of recombination between major circulating clades. J Virol 80(19):9850–9860.
41. Grose C, Brunel PA (1978) Varicella-zoster virus: Isolation and propagation in human melanoma cells at 36 and 32 degrees C. Infect Immun 19(1):199–203.
42. Moffat JF, et al. (1998) The ORF47 and ORF66 putative protein kinases of varicella-zoster virus determine tropism for human T cells and skin in the SCID-hu mouse. Proc Natl Acad Sci USA 95(20):11969–11974.
43. Isler JA, Skalet AH, Alwine JC (2005) Human cytomegalovirus infection activates and regulates the unfolded protein response. J Virol 79(11):6890–6899.

Buckingham et al.